JOURNAL OF SOLID STATE CHEMISTRY 114, 369–378 (1995)

Ordering Principles and Defect Structure of "1201," "1212," and "1222" Type (Hg,Pr)–Sr–(Sr,Ca,Pr)–Cu–O Superconductors

G. Van Tendeloo,*,†,[1] M. Hervieu,* X. F. Zhang,† and B. Raveau*

*Laboratoire CRISMAT, ISMRA and Université de Caen, 6 boulevard du Maréchal Juin, 14050 Caen Cedex, France; and †EMAT, University of Antwerp (RUCA), Groenenborgerlaan 171, B-2020 Antwerp, Belgium

Received October 29, 1993; in revised form April 29, 1994, accepted May 2, 1994

The new families of superconducting compounds "1201" ($Hg_{0.4}Pr_{0.6}Sr_2CuO_{4+\delta}$), "1212" ($Hg_{0.4}Pr_{0.6}Sr_2(Ca_{1-x-y}Sr_xPr_y)Cu_2O_{6+\delta}$), and "1222" ($Hg_{0.4}Pr_{0.6}Sr_2(Pr_{1.7}Sr_{0.3})_2Cu_2O_{8+\delta}$) all show ordering between praseodymium and mercury in the $(Hg,Pr)O_\delta$ plane, reducing the symmetry from tetragonal to orthorhombic or even to monoclinic. In the 1201 compound the ordered superstructure can be described as O_I ($a_I \approx 2a_p$, $b_I \approx a_p$, $c_I \approx c_{1201}$). In the 1212 compound two distinct superstructures are identified, O_I ($a_I \approx 2a_p$, $b_{II} \approx a_p$, $c_I \approx c_{1212}$) and O_{II} ($a_{II} \approx 2a_p$, $b_{II} \approx a_p$, $c_{II} \approx 2c_{1212}$). In some compounds, such as $Hg_{0.4}Pr_{0.6}Sr_2(Ca_{0.4}Sr_{0.4}Pr_{0.2})Cu_2O_{6+\delta}$, the Hg–Pr ordering is only present in microdomains, but due to an ordering between Sr layers and Ca layers, the *c*-axis doubles and one obtains a tetragonal superstructure T_{III} ($a_{III} \approx a_p$, $c_{III} \approx 2c_{1212}$). In the 1222 compound, ordering in the $(Pr,Hg)O_\delta$ plane is very defective; a large number of translation defects actually reduce the symmetry to triclinic.

INTRODUCTION

After the discovery of superconductivity at 94 K in the 1201 type $HgBa_2CuO_{4+\delta}$ superconductor (1), different experiments have been made to try to increase T_c in higher order members of the series "1 2 $n-1$ n." Schilling *et al.* (2), Putilin *et al.* (3), and Antipov *et al.* (4) have shown that for the 1212, 1223, and 1234 members, critical temperatures up to 134 K can be obtained. Under high oxygen pressures, this T_c can even be increased above 150 K (5).

Other experiments have tried to replace Hg with other isovalent or aliovalent ions; they have led to the discovery of a number of new superconducting materials based on the 1201 stacking, $Hg_{0.5}Bi_{0.5}Sr_{2-x}La_xCuO_{4+\delta}$ (6), $Hg_{0.4}Pr_{0.6}Sr_{2-x}Pr_xCuO_{4+\delta}$ (7), and $Hg_{0.3}Pb_{0.7}Sr_{2-x}La_xCuO_{4+\delta}$ (7), characterized by T_c values ranging from 27 to 41 K. The 40 K superconductor $Tl_2HgBa_4Cu_2O_{10+y}$ (8), which corresponds to a regular intergrowth of 2201 type layers $[Tl_2Ba_2CuO_6]_\infty$ with 1201 type layers $[HgBa_2CuO_{4+y}]_\infty$, can also be classified in this series. A second series of mercury-containing cuprates is based on the 1212 type structure. In addition to the 90 K superconductor $(Pb,Hg)Sr_2(Ca,Y)Cu_2O_7$ (9), other superconducting cuprates have been recently isolated: $Hg_{1-x}M_xBa_2Y_{0.6}Ca_{0.4}Cu_2O_{6+\delta}$, ($M$ = Ca, Cu) (T_c = 90 K), (10), $Hg_{1-x'}Ba_2Nd_{1-x}Ca_xCu_{2+x'}O_{6+\delta}$ (T_c = 110 K) (11), and $Hg_{0.5}Bi_{0.5}Sr_2Ca_{1-x}R_xCu_2O_{6+\delta}$, ($T_c$ = 94 K) (12). Recently we have also been able to introduce superconductivity at temperatures up to 85 K in a (Hg–Pr) 1212-based compound (13). During the study of different (Hg–Pr) superconductors (1201 as well as 1212 based) (7, 13) we have found various ordered structures, which we will discuss here in detail. We have also (successfully) tried to introduce other elements such as Pb into the (HgO_δ) plane, but no ordering between Pb and Hg was found.

STRUCTURAL CONSIDERATIONS

The structures, termed "1201," "1212," and "1222," are represented schematically in Figs. 1a–1c. Detailed descriptions of these structures and details regarding the coordination and the layering can be found in (14, 15); specific data for the Hg compounds can be found in (1, 2, 16). Both the 1201 and the 1212 type mercury-based structures can be described in a primitive tetragonal unit cell with respective lattice parameters $a_{1201} \approx a_p \approx 3.8$ Å, $c_{1201} \approx 9.5$ Å, and $a_{1212} \approx a_p \approx 3.8$ Å; $c_{1212} \approx 12.2$ Å; the index p refers to the perovskite type structure. The 1222 structure on the other hand has an *I*-centered space group (*I4/mmm*) due to the presence of a double fluorite type layer between the copper pyramidal layers. Its approximate lattice parameters are $a_{1222} \approx a_p \approx 3.8$ Å, $c_{1201} \approx 30$ Å. Note that when passing from 1201 to 1212 and further to 1222, the distance between successive HgO_δ layers increases from 9.5 to 12.2 to 15.0 Å.

In all of these structures we will study the effect of praseodymium on the mercury sublattice; it will give rise to ordering between both cations.

[1] To whom correspondence should be addressed at EMAT, University of Antwerp (RUCA), Groenenborgerlaan 171, B-2020 Antwerp, Belgium.

0022-4596/95 $6.00

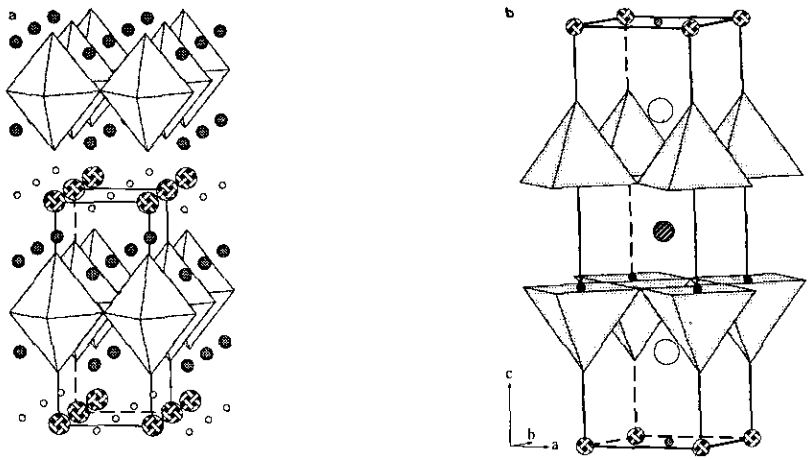

FIG. 1. Schematic representation of the crystal structures of (a) 1201, (b) 1212, and (c) 1222, Hg or Tl positions are represented as the large striped circles; Ba or Sr positions as larger shaded circles; copper atoms are indicated by small black dots. CuO_6 octahedra or CuO_5 pyramids are shaded.

EXPERIMENTAL

The samples with nominal compositions $Hg_{0.4}Pr_{0.6}Sr_2CuO_{4+\delta}$ and $Hg_{0.4}Pr_{0.6}Sr_2(A_{1-x}Pr_x)Cu_2O_{6+\delta}$ (A = Sr, Ca) were prepared from mixtures of HgO, Pr_6O_{11}, SrO_2, $SrCuO_2$, and CaO intensively ground in an agate mortar, according to the above formulas; for the preparation of the compound $Hg_{0.4}Pr_{0.6}Sr_2(Pr_{1.7}Sr_{0.3})_2Cu_2O_{8+\delta}$ we refer to (17). The nominal oxygen content was modified by varying the $SrO_2/SrCuO_2$ ratio. The samples were heated to 800°C in a silica tube; after a plateau of several hours, the temperature was slowly decreased to room temperature.

Samples suited for electron microscopy were obtained by crushing some material in alcohol and depositing flakes on a holey carbon grid. In order to be able to perform microanalysis measurements on these samples, the grids chosen were nickel or aluminum. The electron diffraction study was carried out on a JEOL 200 CX electron microscope equipped with an eucentric goniometer (±60°). High-resolution electron microscopy (HREM) was performed at a TOPCON 002 B microscope, operating at 200 kV, with a point resolution of 1.8 Å. The microanalysis (EDS) was made with a KEVEX analyzer. High-resolution image simulations were performed using the Mac Tempas program.

RESULTS AND DISCUSSION

Ordering in the 1201 Compound

Different initial compositions $Hg_{1-x}Pr_xSr_2CuO_{4+\delta}$ were prepared; however, EDX measurements inside the electron microscope showed that for praseodymium-containing crystals, the cation ratio Hg/Pr always remained more or less constant, with Hg/Pr $\approx \frac{2}{3}$. We therefore concentrated our study on samples with the compositions $Hg_{0.4}Pr_{0.6}Sr_2CuO_{4+\delta}$ and $Hg_{0.5}Pr_{0.5}Sr_2CuO_{4+\delta}$. Actually very few differences were noted between these two compounds.

The electron diffraction patterns of Fig. 2 along the basic sections [001], [100], and [010] confirm the 1201 type structure, but at the same time they show superstructure reflections at positions $\frac{1}{2}$ 0 0, indicating a doubling of the a-axis, but not of the b-axis. The crystal symmetry therefore decreased from tetragonal to orthorhombic. Using X-ray diffraction we confirmed the orthorhombic cell of the structure and determined the lattice parameters of the doubled unit cell as a = 7.606 Å, b = 3.683 Å, c = 8.881 Å (7); we will call this superstructure O_I. The orthorhombicity is $a/2b$ = 1.033; this can be measured directly from the [001] diffraction pattern, but it is even more appealing when the [001] pattern is recorded from two different orientation variants with a common c-axis related by (110) twinning; such a pattern is reproduced in Fig. 2b. The unsplit row of reflections has been indicated, and the spot splitting increases linearly with the distance to the [110]* axis. Similar diffraction patterns have been observed earlier in oxygen-deficient $YBa_2Cu_3O_{7-\delta}$ ($0.3 \leq \delta \leq 0.5$) and have been interpreted to be due to an ordering between oxygen and vacancies in the CuO(1) plane (18, 19). However, in that case the superstructure reflections were very much weaker and more diffuse.

In order to elucidate the nature of the superstructure, we performed HREM along the [010] and [001] directions,

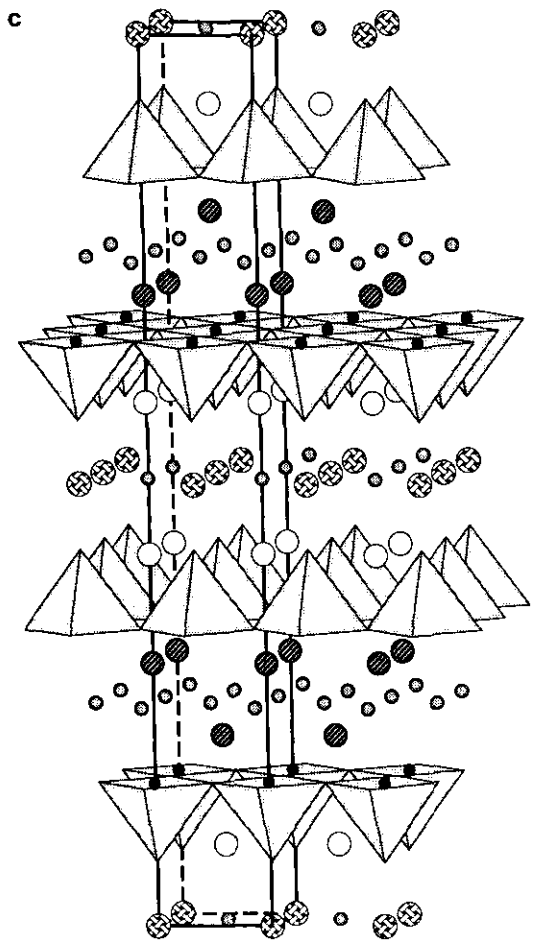

FIG. 1.—*Continued*

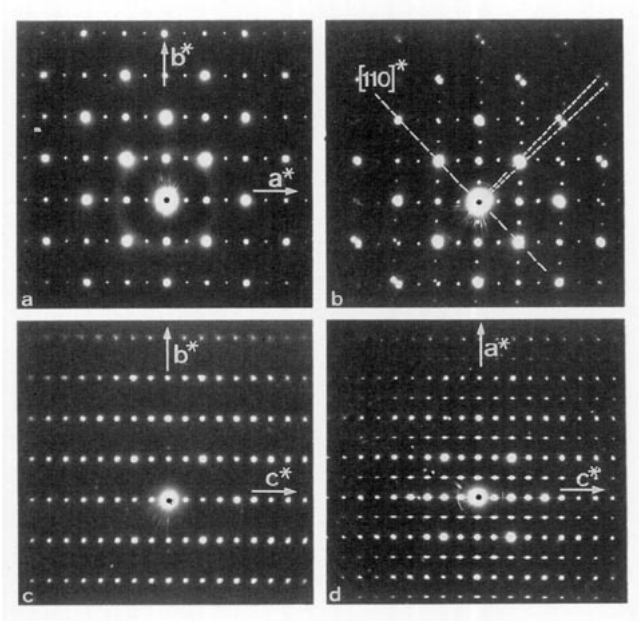

FIG. 2. Electron diffraction patters of $Hg_{0.4}Pr_{0.6}(Sr_{2-x}Pr_x)CuO_{4+\delta}$ along different reciprocal zone axes: (a) along [001] for a single orientation variant; (b) along [001] for two orientation variants related by a (110) mirror operation (note the spot splitting parallel to [110]* due to the orthorhombicity); (c) along [100], no extra reflections are present; and (d) along [010], the doubling along the *a*-axis is clearly visible.

since those sections contain the superstructure reflections. The [001] image in Fig. 3 does show the doubled unit cell along the *a*-axis, particularly in the thicker crystal parts. It is impossible, however, to determine the reason for the cell doubling, since along this projection direction atoms of different nature superimpose; i.e., the projected atom columns do not contain only a single chemical species. Due to the orthorhombic distortion of a tetragonal lattice, coherent (110) twinning does occur, but not in a systematic and pseudoperiodic way as in $YBa_2Cu_3O_{7-\delta}$. Moreover, the twin interfaces are not strictly confined to the (110) plane (see Fig. 3), and the ordering does not fade out under the influence of the electron beam. This suggests that, contrary to the case of $YBa_2Cu_3O_{7-\delta}$, the ordering is not related to the oxygen-vacancy arrangement. In the [010] image of Fig. 4, cell doubling is visible in the thicker parts of the crystal and the doubling is clearly located in the $(Hg,Pr)O_\delta$ plane. The following evidence points toward an ordering of Hg and Pr along the [100] axis in the (001) plane: the fact that in the ideal 1201 structure the oxygen is located at $\frac{1}{2}\ \frac{1}{2}\ 0$; that the superstructure does not vary with oxygen content; that the ordering observed is not influenced by electron irradiation; and that the contrast in the HREM images is rather strong. A structure compatible with all these data is represented schematically in Fig. 5.

The ordering idea is confirmed by the image calculations

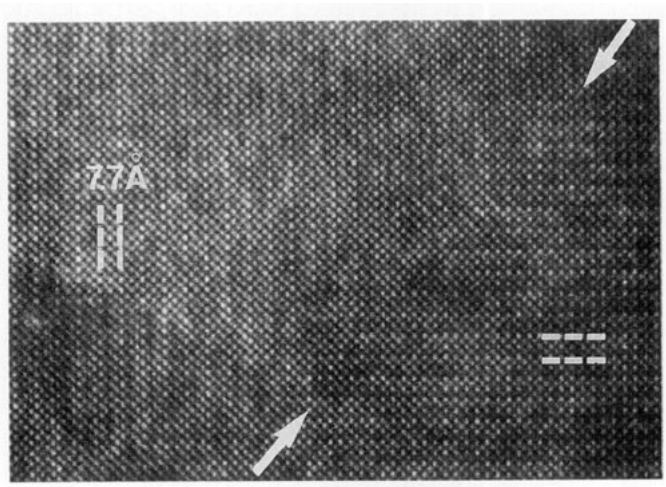

FIG. 3. High resolution image of $Hg_{0.4}Pr_{0.6}(Sr_{2-x}Pr_x)CuO_{4+\delta}$ along [001]; two orientation variants related by a (110) mirror operation are clearly observed.

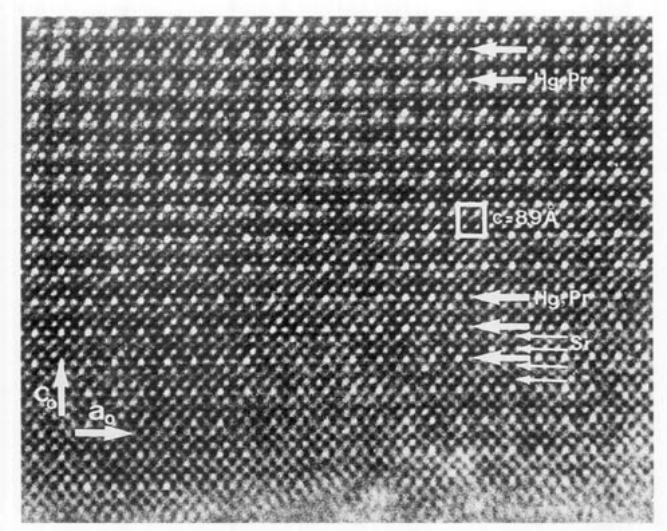

FIG. 4. [010] HREM image of $Hg_{0.4}Pr_{0.6}(Sr_{2-x}Pr_x)CuO_{4+\delta}$; the ordering is observed at the level of the $(Hg,Pr)O_\delta$ plane.

based on the previous assumption; the results are reproduced in Figs. 6 and 7 for an electron incidence along [001] and along [010]. The resemblance with the experimental images is remarkable. For these calculations all atom positions have been left unaltered, and we have introduced an ordering of mercury and praseodymium. We do not know the valence of Pr (Pr^{3+} or Pr^{4+}) nor the exact oxygen content in the plane; however, we have done image simulations for two extreme cases, the oxygen position in the $(Hg,Pr)O_\delta$ plane when fully occupied and the oxygen position when completely empty. The simulated HREM images hardly show any difference. The [001] simulated images confirm the fact that the ordering along this zone is hardly observable in thin areas; because of the mixed columns along this direction, one needs to look into thicker areas (>10 nm) to see an appreciable ordering (Fig. 6). In the simulated [010] images too, the ordering is more pronounced for crystal thicknesses exceeding 10 nm. The Pr columns appear as the darker dots (for $\Delta f = 0$) or as the brighter dots for $\Delta f = -30$ nm (Fig. 7).

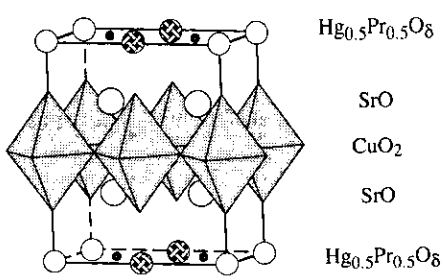

FIG. 5. Schematic representation of the O_I superstructure observed in 1201-type $Hg_{0.4}Pr_{0.6}(Sr_{2-x}Pr_x)CuO_{4+\delta}$; the unit cell is outlined.

Whenever the ordering between Pr and Hg is not perfect, ordering defects such as antiphase boundaries may occur. Because of the doubling of the unit cell along the *a*-axis, the displacement vector of such translation defects will imperatively be $R = \frac{1}{2}[100]$ in the new O_I unit cell. In the HREM image of Fig. 8a several such defects are present; they show a tendency to occur in the (001) planes. The displacement vector $R = \frac{1}{2}[100]_{O_I}$ can be immediately deduced from the higher magnification of Fig. 8b. The ordering, however, is perfect over relatively large areas, which differ from the situation to be discussed in the 1212 and the 1222 systems.

Ordering in the 1212 Compound

In the 1212 family of compounds two different solid solutions have been investigated:

(i) $Hg_{0.4}Pr_{0.6}Sr_2(Sr_{1-x}Pr_x)Cu_2O_{6+\delta}$ with $0.2 \leq x \leq 0.7$; and

(ii) $Hg_{0.4}Pr_{0.6}Sr_2(Ca_{1-x}Pr_x)Cu_2O_{6+\delta}$ with $0.2 \leq x \leq 0.7$

These compositions are local compositions and are determined *in situ* by EDX measurements on the sample characterized by electron diffraction. Similar to the 1201 structure, the rocksalt layer is partially occupied by mercury and praseodymium; the [*A*] layers sandwiched between the pyramidal copper layers are occupied by (Pr, Sr) and (Pr, Ca) respectively (see Fig. 1b). Details on the preparation, as well as on the chemical and physical aspects of these materials can be found in (13).

The electron diffraction study confirmed the basic 1212 structure, but at the same time revealed the presence of several ordering reflections. Two distinct ordering pat-

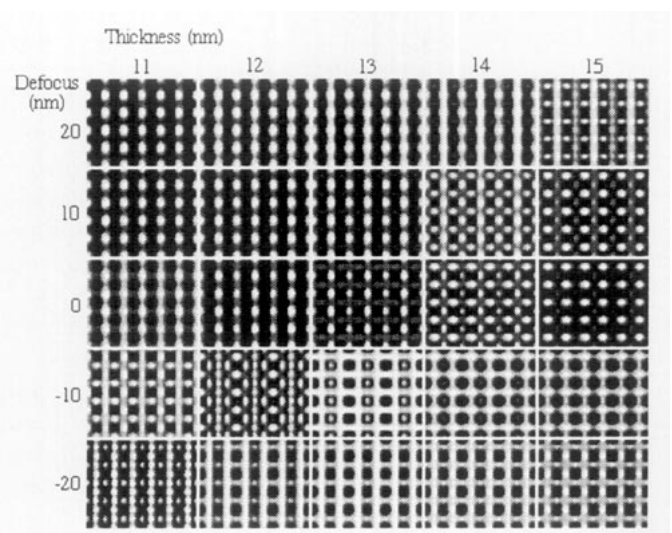

FIG. 6. Simulated [001] HREM images for different defocus values (-20 nm $\leq \Delta f \leq 20$ nm) and different crystal thicknesses between 11 and 15 nm.

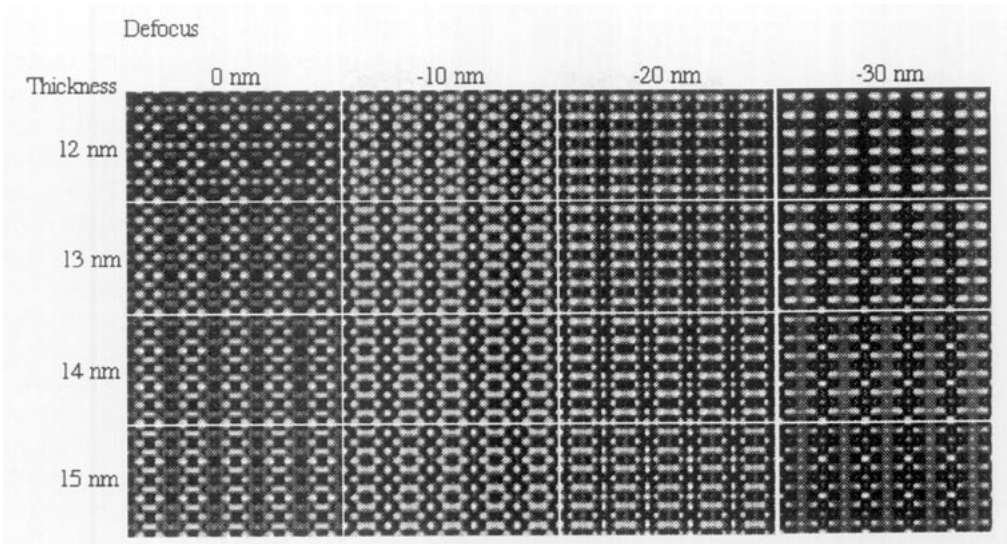

FIG. 7. Simulated [010] HREM images for different defocus values; only part of a complete matrix with $-90\ \text{nm} \leq \Delta f \leq 20\ \text{nm}$ and crystal thickness between 1 and 25 nm is reproduced here.

terns could be observed; they occur with equal probability and sometimes in neighboring areas within the same 1212 grain. Their diffraction patterns are reproduced in Figs. 9a and 9b, respectively.

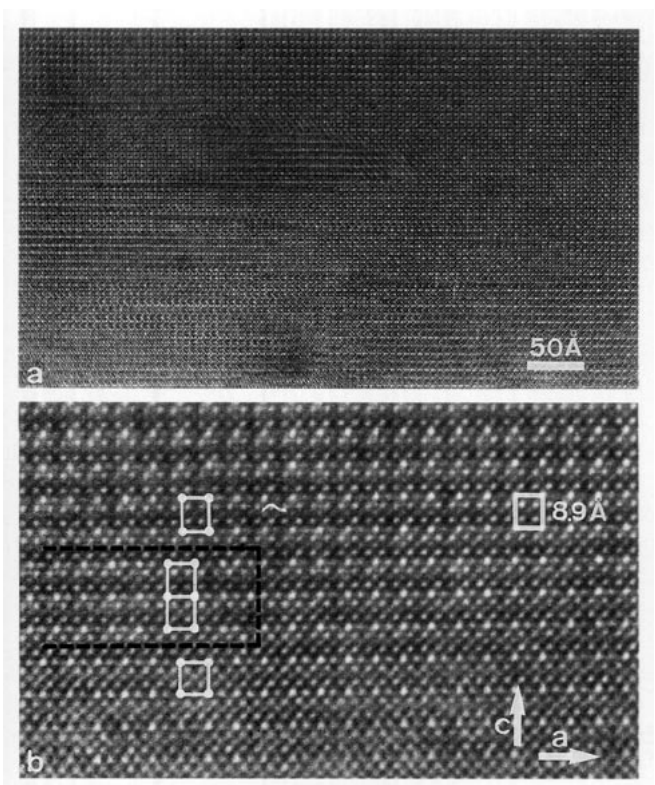

FIG. 8. [010] HREM image of $Hg_{0.4}Pr_{0.6}(Sr_{1.7}Pr_{0.3})CuO_{4+\delta}$. (a) At lower magnification several translation defects are observed. (b) At high magnification the displacement vector R can be immediately deduced; the unit cell is outlined.

The first superstructure, termed O_I, (Fig. 9a) is very similar to the pattern in the 1201 structure (apart from a difference in the length of the c-axis). The structure is orthorhombic and its unit cell is doubled along the a-axis. Also in this case (110) twinning is frequently observed, producing a pseudofourfold symmetry in the [001] diffraction patterns. The $a/2b$ ratio, measured by X-ray and electron diffraction, is equal to 1.01 and is appreciably smaller than that in the 1201 case. This lower $a/2b$ ratio is not surprising, since the distance between successive $(Hg,Pr)O_\delta$ planes increased.

The second superstructure, termed O_{II}, shows superstructure reflections at positions $\frac{1}{2}\ 0\ \frac{1}{2}$ with respect to the basic 1212 structure; they can be appreciated in the [010] diffraction pattern of Fig. 9b. In contrast with the O_I reflections, the O_{II} ordering spots are almost invariably streaked along the c^*-axis, indicating a high degree of planar disorder along the c-axis. A systematic study of reciprocal space revealed an I-centered unit cell with lat-

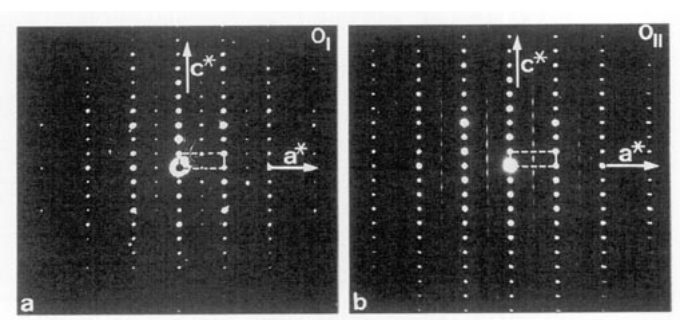

FIG. 9. [010] diffraction pattern of $Hg_{0.4}Pr_{0.6}Sr_2(A_{1-x}Pr_x)Cu_2O_{6+\delta}$: (a) the O_I superstructure; (b) the O_{II} superstructure. The basic "1212" unit has been indicated in both patterns.

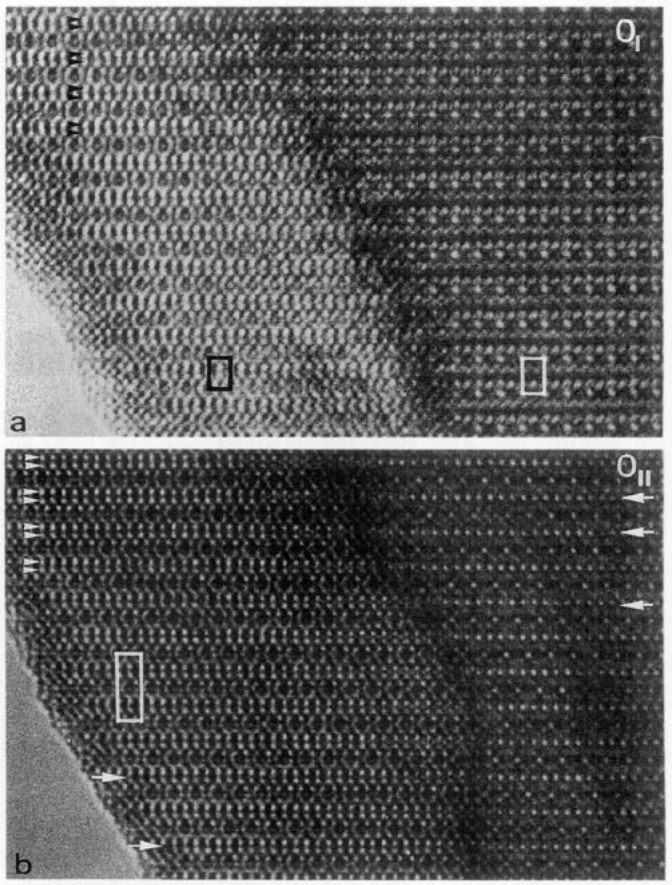

FIG. 10. (a) [010] HREM of the O_I superstructure. The $2a \times c$ unit cell has been outlined. (b) [010] HREM of the O_{II} superstructure. The ordering is clearly visible under a different contrast in the thinner and in the thicker part of the crystal. Double CuO_2 layers are imaged as bright dots and are indicated by double arrowheads; the $2a \times 2c$ unit cell has been outlined. Antiphase boundaries have been indicated by white arrows.

tice parameters $a_{II} \approx 2a_p$, $b_{II} \approx a_p$, $c_{II} \approx 2c_{1212}$, with the reflection conditions $h + k + l = 2n$ being consistent with the $I2/mmm$ symmetry.

High-resolution images (e.g., Fig. 10) indicate that also in the 1212 system the ordering is located in the $(Hg,Pr)O_\delta$ planes. Within a single $(Hg,Pr)O_\delta$ plane the ordering is similar in the O_I and the O_{II} structures; i.e., along the a-axis the Pr and Hg ions alternate. The difference between the two structures is in the stacking along the c-axis of such planes. In the O_I structure successive ordered $(Hg,Pr)O_\delta$ planes are aligned along the c-axis, i.e., the $2a$ unit cell is primitive orthorhombic (Fig. 11a). In the O_{II} structure, however, successive $(Hg,Pr)O_\delta$ planes are staggered and along the c-axis; a Pr position alternates with a Hg position (Fig. 11b). The formation energy for both structures must be very similar, since regions with O_I and O_{II} ordering sometimes occur next to each other, within the same basic 1212 crystal. The O_I ordering is in general rather perfect; ordering defects such as antiphase boundaries are only occasionally observed. The O_{II} ordering, on the other hand, is mostly very defective, a large number of (001) type antiphase boundaries with displacement vector $R = \frac{1}{2}[100]_{O_{II}}$ are present; some of them have been indicated by white arrows in the HREM image of Fig. 10b. Such defects are responsible for the streaking of the ordering reflections along c^* (Fig. 8b).

Image calculations have been performed for both ordering systems O_I and O_{II} in the 1212-based structures (Fig. 12a and 12b). For this model we have taken the atom positions of the average structure as given in (13) and replaced, in an ordered way, half of the mercury ions by praseodymium ions. We have calculated a complete matrix with thickness variations z, 1 nm $\leq z \leq$ 25 nm and focus values Δf, $+20$ nm $\leq \Delta f \leq -100$ nm.

The results confirm the Hg $\leftrightarrow$ Pr ordering principle and allow one to associate the darker dots in Fig. 10 with the Pr ion positions. Again the ordering is best visible for crystal thicknesses exceeding 10 nm. However, a perfect fit between the calculated images and the experimental ones could never be obtained over a large defocus range. This probably means that the real structure deviates slightly from the proposed one. Actually this is not surprising, taking into account that we have simply replaced a bivalent mercury ion by a tri- or tetravalent praseodymium ion without changing the interatomic distances. Moreover the actual composition is $Hg_{0.4}Pr_{0.6}$ rather than $Hg_{0.5}Pr_{0.5}$, which means that some of the Pr has to be distributed statistically on the Hg sublattice. We have failed to prepare the pure stoichiometric $Hg_{0.5}Pr_{0.5}$ composition; this material is apparently not stable, and one always obtains the $Hg_{0.4}Pr_{0.6}$ compound together with some mercury-rich side products.

In compounds with composition $Hg_{0.4}Pr_{0.6}Sr_2(Ca_{0.4}Sr_{0.4}Pr_{0.2})Cu_2O_{6+\delta}$ a completely different type of ordering has been observed, independent of the ordering in the $(Hg,Pr)O_\delta$ plane. The [100] diffraction pattern is shown in Fig. 13; weak superstructure reflections, streaked along c^*, occur at all positions $h\ k\ \frac{1}{2}$, indicating a primitive unit cell, but a doubling of the c-axis (see arrows in Fig. 13). Ignoring the eventual ordering in the $(Hg,Pr)O_\delta$ Plane, the structure remains tetragonal, but with a double c-axis; we will term this structure T_{III} ($a_{III} \approx a_p$, $c_{III} \approx 2c_{1212}$). Such a superstructure with a double c-axis, but with $a_{III} \approx a_p$, cannot be due to ordering within any (001) plane. HREM images from thin crystal parts (Fig. 14a) do not provide much more information, because there is hardly any difference in the images from the ideal 1212 structure, and a doubling of the c-axis is not observed in the thinnest parts (Fig. 14a). In the thicker parts (Fig. 14b and 14c) the doubling of the unit cell is effectively present and located at the $(Ca_{0.4}Sr_{0.4}Pr_{0.2})O_\delta$ plane. Note that the im-

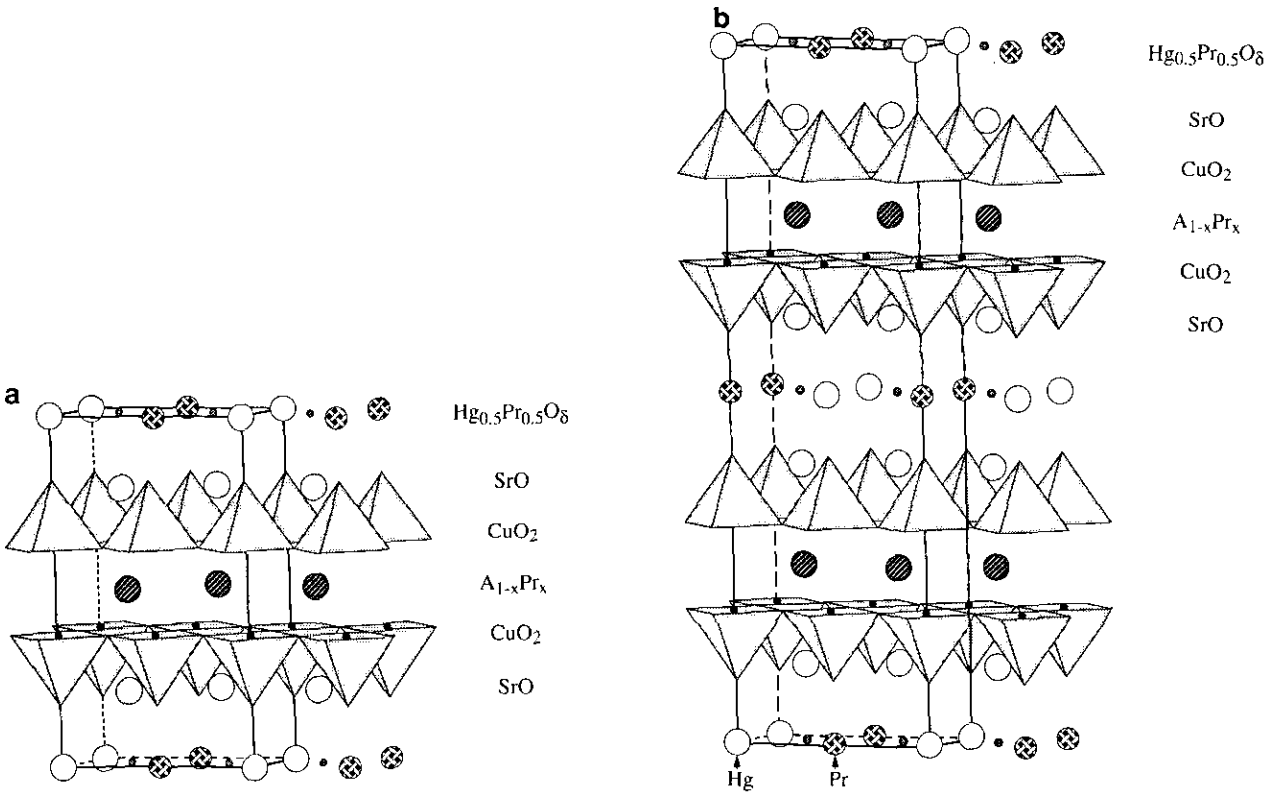

FIG. 11. Schematic representation of the superstructures in $Hg_{0.4}Pr_{0.6}Sr_2(A_{1-x}Pr_x)Cu_2O_{6+\delta}$: (a) the O_I superstructure; (b) the O_{II} superstructure. The unit cell of both superstructures is outlined.

ages in Fig. 14a–14c are taken from the same crystal, at the same defocus value (the same negative!), only at different thicknesses. The only possibility, in agreement with the diffraction data as well as with the HREM data, is to assume that $(Ca_{1-x}Pr_x)O_\delta$ planes alternate with $(Sr_{1-x}Pr_x)O_\delta$ planes along the c-axis. Computer-simulated images for $x = 0$ are shown in Fig. 15; they confirm that the ordering is virtually invisible for thicknesses below 10 nm; their contrast increases with increasing thickness. Moreover, the visibility of the Ca–Sr ordering is highly focus-dependent.

The alternation of Ca and Sr layers is not always obeyed, and several stacking errors occur, explaining the c^* streaking of the superstructure reflections in the diffraction pattern of Fig. 13. Some of these stacking errors are indicated in Fig. 14c. A long white bar or "2" is used

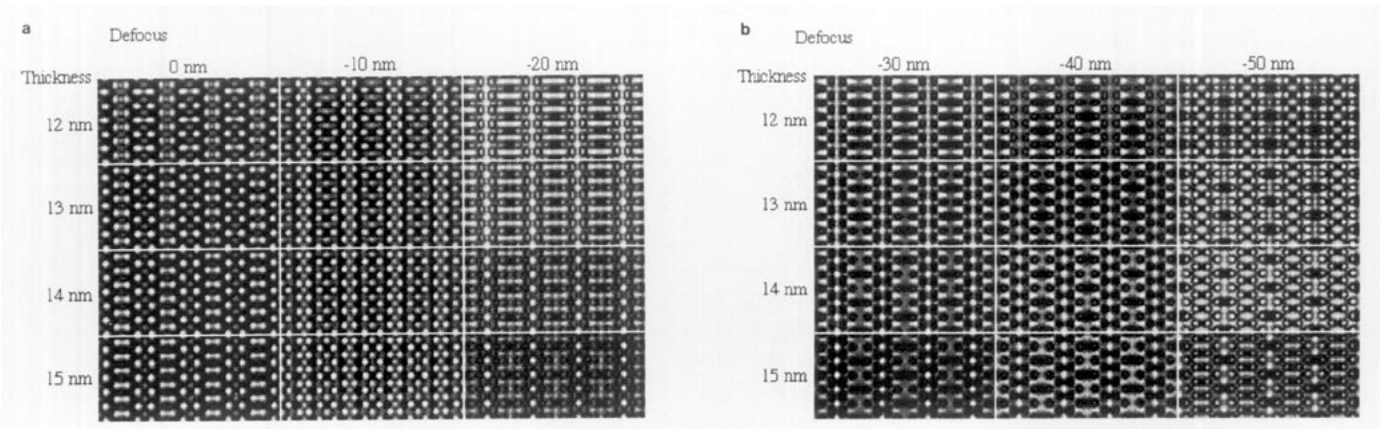

FIG. 12. Calculated [010] HREM images for different defocus values and different thicknesses for (a) the O_I superstructure; (b) the O_{II} superstructure.

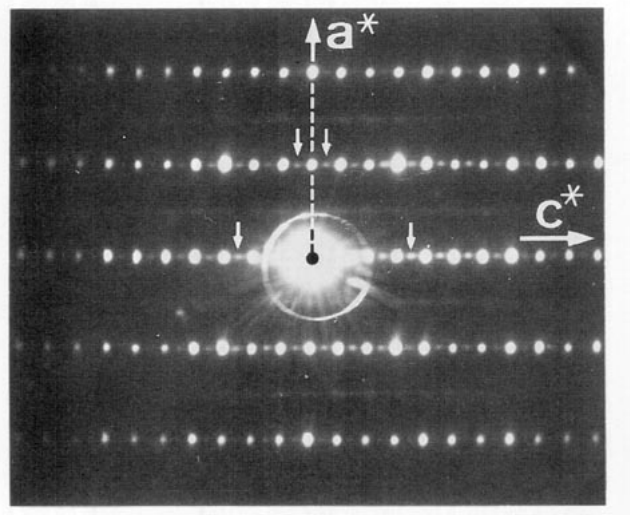

FIG. 13. [010] diffraction pattern of a compound with composition $Hg_{0.4}Pr_{0.6}Sr_2(Ca_{0.4}Sr_{0.4}Pr_{0.2})Cu_2O_{6+\delta}$ where apart from a weak ordering in the $(Hg,Pr)O_\delta$ plane also a doubling of the c-axis is observed. The $\frac{1}{2}[001]_{1212}$ type reflections, indicated by small arrows, cannot be attributed to double diffraction.

for the perfect Ca–Sr alternation; a short bar or "1" is used whenever the alternation is violated and two identical layers are adjacent to each other.

Ordering in the 1222 Compound

In the 1222 family of compounds we have concentrated our efforts on the composition $Hg_{0.4}Pr_{0.6}Sr_2(Pr_{1.7}Sr_{0.3})Cu_2O_{8+\delta}$ where we could also expect an ordering within the $(Hg,Pr)O_\delta$ plane as well as between successive $(Hg,Pr)O_\delta$ planes; the distance between successive ordered planes, however, being approximately 15 Å, was larger than for the previous compounds. Electron diffraction patterns, particularly the [010] pattern (Fig. 16), confirm the 1222 stacking (15, 17). Amazingly there are very few stacking errors compared to the Tl- or Pb-based 1222 cuprates. However, the diffraction patterns reveal a pronounced streaking parallel to [001]*, running halfway between the rows of basic reflections; only very weak maxima can be found at the positions corresponding to the O_{II} structure. This diffuse intensity is compatible with a cell doubling along the a-axis *within* the $(Hg,Pr)O_\delta$ planes, but such that the correlation between successive $(Hg,Pr)O_\delta$ planes is largely lost. High-resolution images along the [010] section reveal the ordering directly (Fig. 17). Particularly in the areas with a crystal thickness between 100 and 200 Å, the copper configuration is imaged as the intense bright dots, while the double Pr layer between two Cu layers is imaged as an almost continuous dark band (see Fig. 17). The $(Hg,Pr)O_\delta$ plane is characterized in this contrast by a series of heavy dark dots, separated by approximately $2a_p$ or 7.6 Å. According to the simulations these dark dots image the Pr configuration with the $(Hg,Pr)O_\delta$ plane. Following a single horizontal line in Fig. 17, one does, however, observe a number of areas where the separation is $3a_p$; i.e., an antiphase shift occurs within a single $(Hg,Pr)O_\delta$ plane. In general the shift is not abrupt but spread over several atomic positions, where a mixed Hg–Pr occupation is present (see the encircled area in Fig. 17). One can argue that, instead of a mixed occupation, the antiphase boundary is inclined with respect to the electron beam; this will in projection also produce mixed columns. In general one can distinguish between both possibilities, because in the latter case, the width of the interface should increase with crystal thickness. In the present situation, however, it is very hard to distinguish between both possibilities, because, as we will see latter, ordering in every individual $(Hg,Pr)O_\delta$ plane is almost independent of the next one; one should therefore introduce the concept of "antiphase line" instead of "antiphase boundary." The situation is somewhat similar to the ordering in $YSr_2CoCu_2O_{7-\delta}$, where we introduced the concept of twin line instead of twin boundary (20). The average distance between successive antiphase lines (within a single $(Hg,Pr)O_\delta$ plane) has been measured for a large number of defects and in a number of crystals; it amounts to $30 \pm 10\ a_{O_1}$ units (i.e., approximately 230 Å). A number of these antiphase lines are indicated in Fig. 17 by vertical arrows.

Due to the presence of the double (Pr,Sr) layer in the basic 1222 structure, equivalent Pr (or Hg) positions cannot be aligned along c in subsequent (Hg,Pr)Oδ planes;

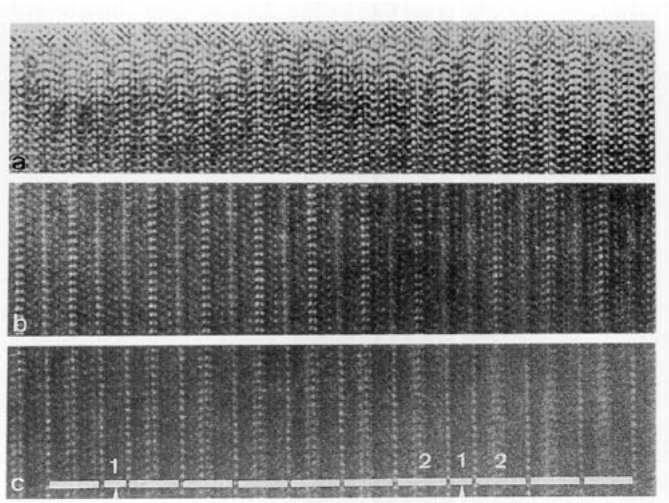

FIG. 14. [010] HREM images of $Hg_{0.4}Pr_{0.6}Sr_2(Ca_{0.4}Sr_{0.4}Pr_{0.2})Cu_2O_{6+\delta}$, corresponding to the diffraction pattern of Fig. 13: (a) in the thinner parts no ordering effects can be distinguished; (b, c) in the thicker parts the distinction between $(Ca_{1-x}Pr_x)O_\delta$ and $(Sr_{1-x}Pr_x)O_\delta$ planes becomes prominent.

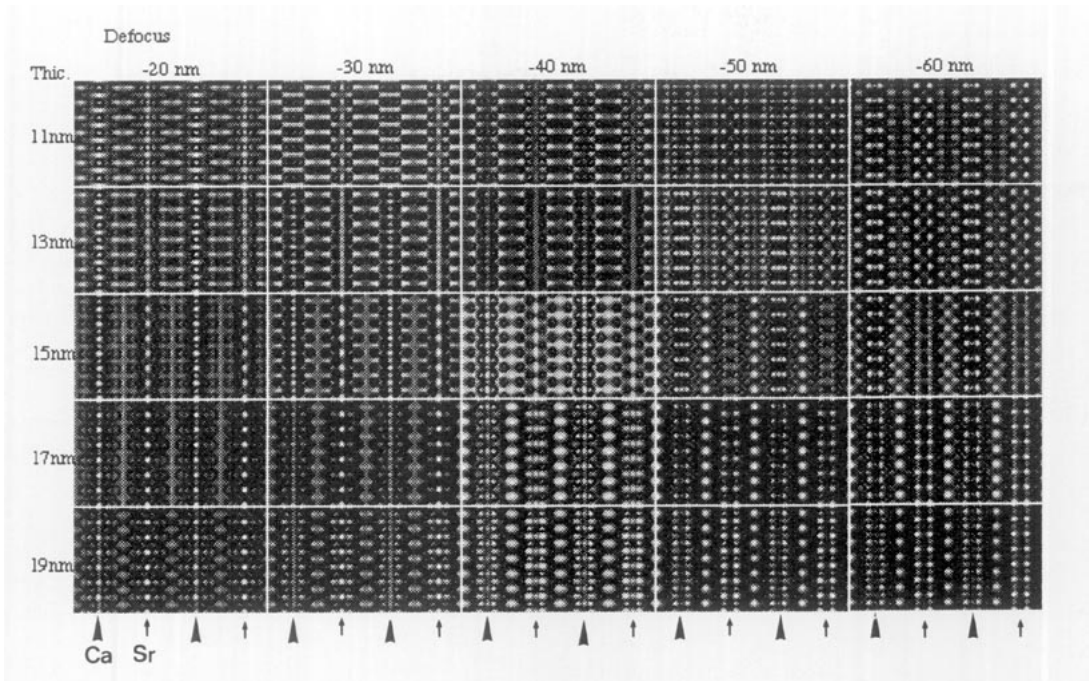

FIG. 15. Calculated [010] HREM images for different defocus values and different thicknesses of the tetragonal T_{III} structure. The positions of the Ca and Sr rows have been indicated.

they are necessarily shifted over $+\frac{1}{2}a_p$ or $-\frac{1}{2}a_p$. The basic 1222 unit cell, without taking into account the Hg ↔ Pr ordering, has been outlined in the lower left corner of Fig. 17. In the present compound, however, Hg ↔ Pr ordering does occur within a single $(Hg,Pr)O_\delta$ plane, but the correlation between successive $(Hg,Pr)O_\delta$ planes is virtually completely lost. Antiphase lines in one $(Hg,Pr)O_\delta$ plane do not necessarily introduce antiphase lines in the next $(Hg,Pr)O_\delta$ plane, which is separated from the preceding plane by about 15 Å. The relation between the ordering in successive $(Hg,Pr)O_\delta$ planes is random and hence it is impossible to maintain an orthorhombic unit cell as in the basic 1222 structure (compare to Fig. 1c). We therefore have to describe the structure as triclinic, with unit cell parameters $a_t = 2a_p$, $b_t = b_p$, $c_t = \frac{1}{2}(c_{1222} + a_p + b_p)$ and angles $\alpha \approx 82.9°$, $\beta \approx 82.9°$, and

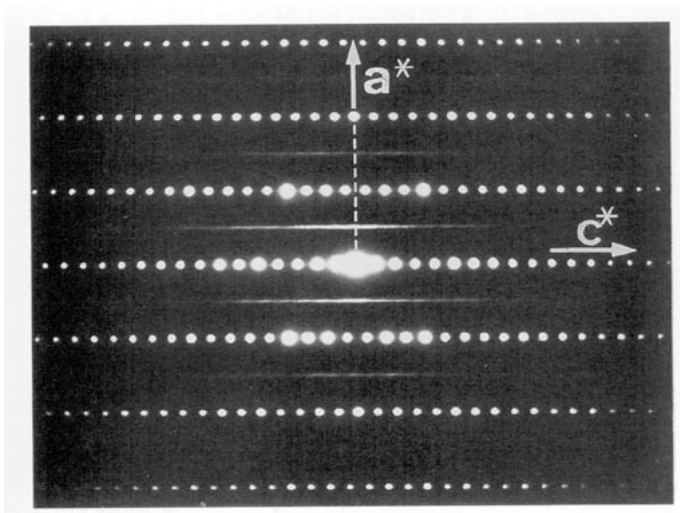

FIG. 16. [010] diffraction pattern of $Hg_{0.4}Pr_{0.6}Sr_2(Pr_{1.7}Sr_{0.3})_2Cu_2O_x$; the basic structure is well defined, while the ordering between Hg and Pr introduces diffuse streaks between basic [001]* rows.

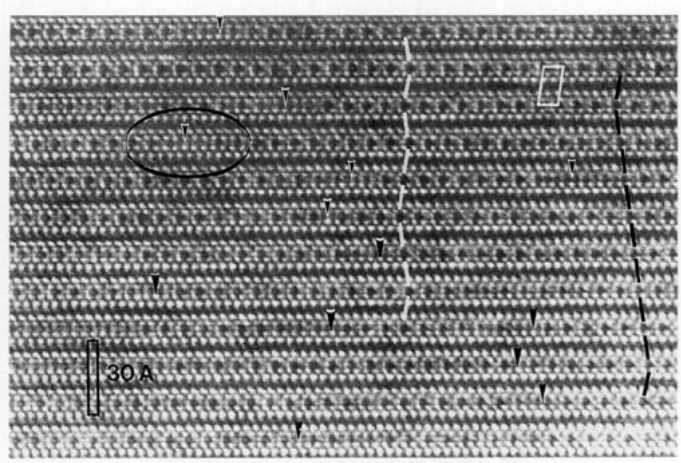

FIG. 17. HREM image of the 1222 compound, corresponding to the diffraction pattern of Fig. 16. The Pr configuration in the $(Ca_{0.4}Pr_{0.6})O_\delta$ plane is imaged as dark dots. The projected basic 1222 unit cell is outlined in black in the lower left corner, while the triclinic unit cell introduced by the in-plane ordering is outlined in the upper right corner. Antiphase lines have been indicated by vertical arrow heads.

$\gamma = 90°$. Projected along the [010] direction, as in Fig. 17, the unit cell is a parallelogram (a_m, c_m) with $a_m = 2a_p$, $c_m = \frac{1}{2}(c_{1222} + a_p)$ and $\beta \approx 82.7°$; this projected unit cell has been indicated in white in the upper right corner of Fig. 17. The defects due to a lack of correlation between successive layers can be described as microscale twinning, the $(Hg,Pr)O_\delta$ planes being the twin planes. The twin sequence in two different parts of the crystal, hardly 100 Å apart, has been indicated in Fig. 17 by the white and black vertical zigzag lines; it is clear from this that it makes no sense to define a superstructure unit cell and that the ordering is best described as a microtwinning of the triclinic structure defined above.

CONCLUDING REMARKS

The ordering in different superconducting materials of the family "1 2 n − 1 n" (with $n = 1, 2$) such as the 1201-type $Hg_{0.4}Pr_{0.6}Sr_2CuO_{4+\delta}$ and the 1212-type $Hg_{0.4}Pr_{0.6}Sr_2(Ca_{1-x-y}Sr_xPr_y)Cu_2O_{6+\delta}$, as well as in the 1222-type $Hg_{0.4}Pr_{0.6}Sr_2(Pr_{1.7}Sr_{0.3})_2Cu_2O_{8+\delta}$, has been studied in detail by electron diffraction and HREM. Within a single $(Pr,Hg)O_\delta$ plane the ordering is the same for all compounds; Pr and Hg atoms alternate along the a_p-axis, destroying the tetragonal symmetry. Depending on the value of n, different superstructures have been found. With increasing distance between the $(Pr,Hg)O_\delta$ planes, the correlation between such planes decreases, and the ordered structure becomes more and more defective. For the 1222 structure, the correlation is almost ocmpletely lost, and the ordered structure has to be described in a triclinic unit cell.

In some compounds of the 1212-type, such as those which contain Ca as well as Sr in the fluorite type cases, (e.g., in $Hg_{0.3}Pr_{0.7}Sr_2(Ca_{0.4}Sr_{0.4}Pr_{0.2})Cu_2O_{6+\delta}$) the Hg ↔ Pr ordering is very limited; but due to an ordering between the Sr layers and Ca layers, the c-axis doubles and the superstructure T_{III} is tetragonal ($a_{III} \approx a_p$, $c_{III} \approx 2c_{1212}$).

All these ordered superstructures indicate that the "1201," "1212," and "1222" frameworks are very tolerant in accepting foreign elements or substitutions into their sublattice, without changing the basic structure. It is very probable that, depending on the substitutions, different superstructures can be found in these compounds.

ACKNOWLEDGMENT

X. F. Zhang is grateful for financial support from the Belgian IUAP 48 Programme.

REFERENCES

1. S. N. Putilin, E. V. Antipov, O. Chmaissen, and M. Marezio, *Nature (London)* **362,** 226 (1993).
2. A. Schilling, M. Cantoni, J. D. Guo, and H. R. Ott, *Nature (London)* **363,** 56 (1993).
3. S. N. Putilin, E. V. Antipov, and M. Marezio, *Physica C* **212,** 266 (1993).
4. E. V. Antipov, S. M. Loureiro, C. Chaillout, J. J. Capponi, P. Bordet, J. L. Tholence, S. N. Putilin, and M. Marezio, *Physica C* **215,** 1 (1993).
5. C. W. Chu, L. Gao, F. Chen, Z. J. Huang, R. L. Meng, and Y. Y. Xue, *Nature* **365,** 323 (1993); M. Nunez-Regueiro, J. L. Tholence, E. V. Antipov, J.-J. Capponi, and M. Marezio, *Science* **262,** 97 (1993).
6. D. Pelloquin, C. Michel, G. Van Tendeloo, A. Maignan, M. Hervieu, and B. Raveau, *Physica C* **214,** 87 (1993).
7. F. Goutenoire, P. Daniel, M. Hervieu, G. Van Tendeloo, C. Michel, A. Maignan, and B. Raveau, *Physica C* **216,** 243 (1993).
8. C. Martin, M. Huvé, G. Van Tendeloo, A. Maignan, C. Michel, M. Hervieu, and B. Raveau, *Physica C* **212,** 274 (1993).
9. S. F. Hu, D. A. Jefferson, R. S. Liu, and P. P. Edwards, *J. Solid State Chem.* **103,** 280 (1993).
10. A. Maignan, G. Van Tendeloo, M. Hervieu, C. Michel, and B. Raveau, *Physica C* **212,** 239 (1993).
11. A. Maignan, C. Michel, G. Van Tendeloo, M. Hervieu, and B. Raveau, *Physica C* **216,** 1 (1993).
12. D. Pelloquin, M. Hervieu, C. Michel, G. Van Tendeloo, A. Maignan, and B. Raveau, *Physica C* **216,** 257 (1993).
13. M. Hervieu, G. Van Tendeloo, A. Maignan, C. Michel, F. Goutenoire, and B. Raveau, *Physica C* **216,** 264 (1993).
14. R. Raveau, C. Martin, M. Hervieu, D. Bourgault, C. Michel, and J. Provost, *Solid State Ionics* **39,** 49 (1990).
15. C. Martin, D. Bourgault, M. Hervieu, C. Michel, J. Provost, and B. Raveau, *Mod. Phys. Lett. B* **3,** 993 (1989).
16. J. L. Wagner, P. G. Radaeli, D. G. Hinks, J. D. Jorgensen, J. F. Mitchell, B. Dabrowski, G. S. Knapp, and M. A. Beno, *Physica C* **210,** 447 (1993).
17. M. Hervieu, C. Martin, G. Van Tendeloo, C. Michel, A. Maignan, and B. Raveau, *J. Solid State Chem.*, in press (1995).
18. G. Van Tendeloo, H. W. Zandbergen, and S. Amelinckx, *Solid State Commun.* **63,** 603 (1987).
19. M. Hervieu, B. Domengès, C. Michel, J. Provost, and B. Raveau, *J. Solid State Chem.* **71,** 263 (1987).
20. T. Krekels, O. Milat, G. Van Tendeloo, S. Amelinckx, T. N. G. Babu, A. J. Wright, and C. Greaves, *J. Solid State Chem.* **105,** 313 (1993).